

## Death and revival of chaos

Bálint Kaszás

*Institute for Theoretical Physics, Eötvös Loránd University, Pázmány Péter Sétány 1/A, H-1117 Budapest, Hungary*

Ulrike Feudel

*Theoretical Physics/Complex Systems, ICBM, Carl von Ossietzky University Oldenburg, 26129 Oldenburg, Germany*

Tamás Tél

*Institute for Theoretical Physics, Eötvös Loránd University, Pázmány Péter Sétány 1/A, H-1117 Budapest, Hungary  
and MTA-ELTE Theoretical Physics Research Group, Pázmány Péter Sétány 1/A, H-1117 Budapest, Hungary*

(Received 22 July 2016; revised manuscript received 18 November 2016; published 28 December 2016)

We investigate the death and revival of chaos under the impact of a monotonous time-dependent forcing that changes its strength with a non-negligible rate. Starting on a chaotic attractor it is found that the complexity of the dynamics remains very pronounced even when the driving amplitude has decayed to rather small values. When after the death of chaos the strength of the forcing is increased again with the same rate of change, chaos is found to revive but with a different history. This leads to the appearance of a hysteresis in the complexity of the dynamics. To characterize these dynamics, the concept of snapshot attractors is used, and the corresponding ensemble approach proves to be superior to a single trajectory description, that turns out to be nonrepresentative. The death (revival) of chaos is manifested in a drop (jump) of the standard deviation of one of the phase-space coordinates of the ensemble; the details of this chaos-nonchaos transition depend on the ratio of the characteristic times of the amplitude change and of the internal dynamics. It is demonstrated that chaos cannot die out as long as underlying transient chaos is present in the parameter space. As a condition for a “quasistatically slow” switch-off, we derive an inequality which cannot be fulfilled in practice over extended parameter ranges where transient chaos is present. These observations need to be taken into account when discussing the implications of “climate change scenarios” in any nonlinear dynamical system.

DOI: [10.1103/PhysRevE.94.062221](https://doi.org/10.1103/PhysRevE.94.062221)

### I. INTRODUCTION

Chaotic dynamics has been celebrated as an important part of different processes in various disciplines of science like mechanics, optics, meteorology, chemistry, neuroscience, and population dynamics, as presented in several textbooks (see, e.g., [1–4]). Macroscopic systems are generally dissipative, and they are driven by external forces in order to compensate energy loss. External drivings are typically assumed to be temporally periodic. The widespread theory of chaos is based on the existence of an infinity of unstable periodic orbits [1–3]. Here we investigate how chaos dies out (and revives) in dissipative systems, under a realistic time-dependent change of parameters, a question not yet studied in the literature. To this end, we pass with a certain speed through a considerable range of the parameter space and enter the region where only simple dynamics is possible (in our illustrative example, even the region where the motion is about to stop). Thus, we have to inevitably leave the traditional theory of chaotic systems, as the time dependence of the driving is not purely periodic, it exhibits a trend and hence no periodic orbits can exist.

In cases when the dynamics is complex, it is not even known what should be understood under chaotic behavior. For example, the widely used concept of Lyapunov exponents, in the traditional formulation, requires a long-term observation, but with shifting parameters, the character of the dynamics also changes, and one should then concentrate on finite temporal intervals, but their particular choice would be a source of subjectivity. Instead of a search for an exact definition, we decide to follow a qualitative picture: we examine for how

long a typical property of chaos holds, namely the coexistence of a wide variety of possible motions, in other words, the internal *variability* of the dynamics. A central observation of our studies is that the variability lasts for surprisingly long periods of time, up to times when the magnitude of driving falls down to rather small values. The linear (and therefore certainly not chaotic) behavior about the state of rest can set in only afterwards. The interest in systems with trends in their parameter change is motivated by the problem of *climate change*, and concerns related to it. Several studies indicate that such a change can lead to qualitative changes in the dynamics:

One branch of research concentrates on bifurcations in various contexts in mathematics, physics, and biology, traversed with a time scale similar to that of the internal dynamics. Bifurcations are found to occur often delayed like in the case of period doubling [5], transcritical bifurcation in lasers [6,7], or Hopf bifurcation [8], and resonances [9], and the observed delay depends on the speed of the parameter change. The literature refers to bifurcation tipping or ramped tipping [10–12], the former denotes the case where a bifurcation is involved in the qualitative change of the dynamics when a parameter is varied in time, while the latter corresponds to crossing manifolds in state space as a consequence of a shift in a parameter. Appropriate mathematical methods to tackle those questions in which the time scale of variation of the parameter is different from the time scale of the internal dynamics are multiscale methods [13]. None of these bifurcation-related studies have ever addressed the question of what happens to bifurcations leading to chaos.

Another branch of research concentrates on changes in chaotic attractors due to parameter changes [14–18]. These studies look at the impact of shifting environmental conditions from a more general perspective to, e.g., reveal the consequences of climate change on the number of extreme events to be expected in the future [17]. Atmospheric motion is often described by chaoticlike dynamics and hence, changes in the shape of chaotic attractors and/or their statistical properties are the result of trends acting on the system. This part of the literature has not addressed the question of the disappearance of chaotic attractors.

Our subject lies thus at the boundary of these different classes of approach. A concept ideally suited to the study of dynamical systems with arbitrary time dependence—and this is what we find appropriate to use in our problem—is that of snapshot attractors [19] (also called pullback attractors in the mathematics and climate-related literature [14, 16, 20–22]). Loosely speaking, a snapshot attractor is an object belonging to a given time instant that is traced out by an *ensemble* of trajectories initialized in a region of the phase space in the past, all of the ensemble members governed by the same equation of motion. In the dynamical systems community, the concept of snapshot attractors has been known and successfully applied for many years [19, 23–29]. A precursor was the discovery of synchronization by common noise (i.e., by the same realization of a random driving) by Pikovsky [30], a case when—in the current terminology—the snapshot attractor turns out to be regular. The use of deterministic driving goes back to Kloeden [21] and to recent climatic applications [18, 31]. By now, applications to systems with a high degree of freedom are also available [32–34].

For our investigation of the dying out (and revival) of chaos we choose a paradigmatic example of a driven dissipative system, a driven pendulum whose suspension is oscillating periodically. With a constant driving amplitude, an extended chaotic attractor is known to exist [2]. In our model this amplitude is assumed to decay in time, but the period of oscillation is unchanged. Thus the possibility of defining a stroboscopic map, often used in the description of usual chaos, is kept, although periodic orbits themselves obviously do not exist any longer. We emphasize, however, that the role of periodicity is not essential, it provides merely a natural sampling time. In other problems with driving without any periodicity such a sampling time can be chosen arbitrarily. The advantage of having periodicity in our problem is, nevertheless, that conventional methods can be applied before the switching off process starts.

As for the temporal change of the driving, we take an exponentially decaying form. An advantage of this is that the driving decays in a similar way as the relaxation caused by dissipation. Both can be characterized by constant relaxation times. The switching off is considered to be fast, if its time constant is smaller than that of dissipation. We are mainly interested in the range where the two times are comparable, but also find a criterion for the case when the switching off process could be considered to be quasistatic.

After introducing the model in the next section (Sec. II), we turn to the presentation of the bifurcation diagram of the original dynamics with time-independent driving amplitudes (Sec. III). The case studies of the system with decaying

amplitude (Sec. IV) indicate that individual trajectories are not representative and motivate us to turn to an ensemble approach. The results related to the geometry of the snapshot attractor and its comparison with that of the attractors of the bifurcation diagram, and with the unstable manifolds of the underlying transient chaos, are summarized in Sec. V. The dynamics' strong variability is shown to be accompanied by a horseshoelike structure in the stable and unstable foliations found to be present also in the dynamics with decaying driving. Next we turn to a statistical characterization of the snapshot attractors in terms of the standard deviation of one of their coordinates and find that a drop in this quantity might be used as a sign of chaos death. In the same Sec. VI we also study the revival of chaos seen when the decay of the driving amplitude is changed into an increase, and find a strongly different history, reflected by a pronounced hysteresis loop in the standard deviation-driving amplitude plane. A summary is given in Sec. VII augmented with a discussion of when a parameter change can be considered to be “quasistatic.” We come to the conclusion that over an extended range of parameters this is practically not possible due to the transient chaos underlying the original problem, a feature never reflected in traditional bifurcation diagrams.

## II. EQUATION OF MOTION

The dimensionless equation of motion for the angle  $\varphi$  taken with respect to the vertical of a driven mathematical pendulum with its suspension point moving periodically along a horizontal line with a constant amplitude  $C$  reads as [2]

$$\ddot{\varphi} = -\gamma^2 \sin \varphi - 2\beta\dot{\varphi} + C \cos(\varphi) \cos(t). \quad (1)$$

The dimensionless driving period is  $T = 2\pi$ , while  $\gamma$  represents the dimensionless frequency of the pendulum's small amplitude swingings without driving and dissipation, and  $\beta$  is a friction constant. In our numerical study we shall fix the values of  $\gamma = 1/3$  (the driving frequency is three times that of the eigenfrequency) and of  $\beta = 0.05$  (the dissipative relaxation rate is 1/20th of the driving frequency).

With dimensionless driving amplitude  $C_0 = 2$ , i.e., when the amplitude of the suspension point's oscillation is twice as large as the length of the pendulum, the dynamics is chaotic and possesses an underlying chaotic attractor of large extension [2].

For simplicity, we model the switching off process by taking the driving amplitude to be the time dependent  $C(t)$  with the following particular exponential scenario:

$$C(t) = \begin{cases} C_0, & \text{for } t < t_0 = 10T, \\ C_0 e^{-\alpha(t-t_0)}, & \text{for } t \geq t_0 = 10T. \end{cases} \quad (2)$$

This corresponds to the situation when the pendulum is driven with a constant amplitude  $C_0 = 2$  up to time  $t_0 = 10T$  (trajectories are found to need much shorter times, about  $3T$ , to reach the chaotic attractor), and at this instant the decay of the amplitude starts with an exponential *switch-off rate*  $\alpha$  as depicted in Fig. 1.

Five different values of  $\alpha$ , 0.2, 0.1, 0.05, 0.025, and 0.0125, are selected for the switching off scenarios. The switch-off rates  $\alpha$  should be compared with the dissipative relaxation rate  $\beta = 0.05$ . The comparison is more illuminating by comparing

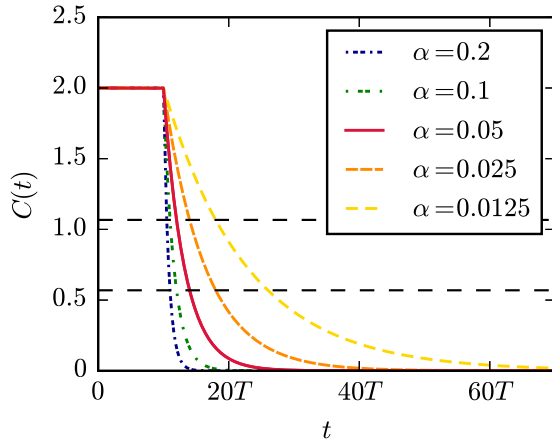


FIG. 1. The investigated switching off scenarios: time dependence of the driving amplitude  $C(t)$  for different switch-off rates  $\alpha$ . Horizontal dotted lines indicate the two  $C$  values,  $C = 1.0670$  and  $C = 0.5692$ , for which the switching off processes with the various switch-off rates are compared later. The other dimensionless parameters used throughout the paper are  $\beta = 0.05$  and  $\gamma = 1/3$ .

the reciprocals, the (dimensionless) relaxation times,  $\tau_d$  and  $\tau_s$ :

$$\tau_d = \frac{1}{\beta} = 20, \quad \tau_s = \frac{1}{\alpha} = 5, 10, 20, 40, 80. \quad (3)$$

Two of the switching off scenarios are thus faster than the relaxation induced by dissipation, one has the same characteristic time as friction (continuous curve in Fig. 1), and two others are slower. We claim to have realistic scenarios with either slower or faster changes in the forcing but still on almost the same order of the time scale of the internal dynamics. To emphasize the contrast with infinitely slow parameter changes, reflected in traditional bifurcation diagrams, scenarios with  $\alpha$  on the order of  $10^{-3}$  or smaller are not considered.

One advantage of our setup is that the relaxation times are constant, independent of other parameters and, in particular, of the instantaneous value of the driving amplitude. (In the case of nonexponential decays only instantaneous dissipative and switch-off rates can be defined.)

Equation (1) with  $C = C(t)$  as given in (2) is solved numerically by means of a fourth order Runge-Kutta method with fixed time step  $h = 0.01T$  or smaller.

### III. STROBOSCOPIC MAPPING AND BIFURCATION DIAGRAMS

For a frozen-in, constant amplitude case with  $C_0 = 2$  a usual chaotic attractor is present with a stroboscopic view as shown in the first panel of Fig. 4. This can be obtained by following a single initial point for a long time and by determining hundred thousands of stroboscopic intersection points. It is worth noting that the frozen-in chaotic attractor can also be obtained in a conceptually different way. One can choose, say, 100 000 points distributed uniformly in a region of the phase space. Plotting the stroboscopic position of all the trajectories after a few, say 10, periods the same figure is reproduced. This is a consequence of the ergodicity of the frozen-in chaotic dynamics.

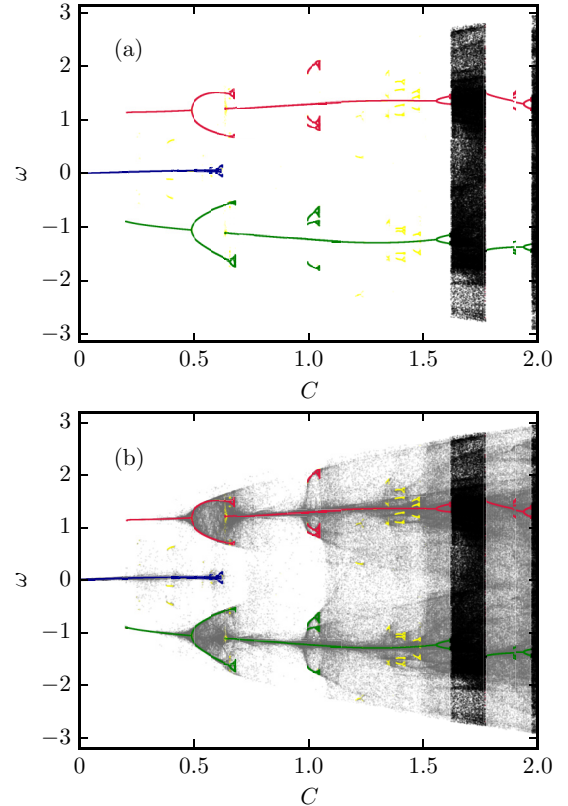


FIG. 2. Bifurcation diagram of the driven pendulum with frozen-in amplitude  $C$ . (a) The  $\dot{\varphi} = \omega$  coordinates on the long-term attractors are plotted in the stroboscopic map. The upper (red), middle (blue) and lower (green) curves indicate the bifurcations of three orbits which are of period 1 for small  $C$ : middle (blue), small amplitude swinging, upper (red), lower (green), clockwise, and counterclockwise overturning motion. The latter are born in a saddle-node bifurcation at  $C = 0.2$ . Small multipiece attractors appear as light (yellow) patches. (b) The angular velocity coordinates during long-lived transients are also shown, colored gray. Note how much more empty the traditional diagram (a) is.

The bifurcation diagram [3,4] of dynamics (1) with different constant driving amplitudes  $C$  has been determined in the range  $(0, 2)$ , as depicted in Fig. 2. The results presented for the angular velocity variable indicate that large, extended chaotic attractors only exist close to  $C = 2$  and in the amplitude range around  $C \in (1.6, 1.8)$ . There are a few other, rather short ranges of  $C$  where chaotic attractors exist but these are small multipiece objects. The bifurcation diagram of the dynamics with frozen-in driving amplitudes is thus dominated by *regular* motion.

The traditional bifurcation diagram of Fig. 2(a) is obtained by plotting the asymptotic coordinates of 400 uniformly distributed points after 1000 periods. A different facet of the dynamics is revealed in Fig. 2(b) by plotting the coordinates after 20 periods only. The results are plotted as gray points. They trace out broad vertical intervals about the periodic attractors (colored dots). The appearance of these intervals is a unique sign of the existence of relatively long transients, most likely of transient chaos preceding the capture of trajectories by the periodic attractors. The plot indicates that unlike permanent

chaos, transient chaos is present in a rather broad range of the frozen-in dynamics: for all  $C$  values larger than about  $C = 0.3$ .

**IV. CASE STUDIES WITH DECAYING AMPLITUDES**

One of the system’s most interesting features is that the motions can be drastically different during the entire switching off process, depending on the initial conditions. To illustrate this, we choose initial conditions in the last moment of the existence of the frozen-in chaotic attractor, at  $t = 10T$ . Significant differences are found during rather long time intervals. This clearly shows that a strong internal variability characterizes the system during most of the switching off process. Despite the fact that the initial conditions differ only slightly, the functions  $\varphi(t)$  and  $\omega(t)$  differ significantly, as shown in Fig. 3. The angle  $\varphi$  is displayed in the interval  $(-\pi, \pi)$ , in a periodic representation. Accordingly, if the curve crosses the boundary, it enters from the bottom, marking an overturning of the pendulum. The motions presented correspond to energy rich initial conditions since overturnings last up to about 25 periods, although details are different. Even more significant differences can be seen in the angular velocity: between periods 15 and 25 both pendula rotate with an approximately constant angular velocity, but these values

are about  $+1$  and  $-1$ , respectively. Small amplitude swinging about the origin sets in after more than 40 periods only, when the driving amplitude has fallen to one-hundredth of its original value. Figure 3 and a number of additional simulations illustrate the high degree of variability of the switching off dynamics. This is of course partly inherited by the chaoticity of the first ten periods, but as the accumulation about  $\omega = \pm 1$  shows, the entire decay process also contributes to the internal variability. Our goal is a more complete exploration of this property.

**V. SNAPSHOT ATTRACTOR VIEW**

According to the analysis in the previous section, a randomly selected switching off trajectory is usually *not representative*. What can be considered to be representative can only be decided when looking at several trajectories simultaneously. Let’s start therefore the investigation of the time evolution of phase-space *ensembles*. Such approach is becoming increasingly popular in the literature on the dynamics of nonautonomous systems with smooth *shifts* in the parameters, like in the dynamics of climate change (see, e.g., [16,18], or in engineering problems [35]). Clearly, in such cases the monitoring of a single long trajectory and the ensemble picture lead to different results: ergodicity does not hold [36]. It is the latter picture which proves to be effective because the ensemble defines, after some time, a distribution, specifying how many members of the ensemble fall close to certain points in phase space, at any given time. The set traced out by the ensemble is called the *snapshot attractor*, which is always subject to temporal change. The attractor itself and the distribution on it are independent of the choice of the initial distribution of the ensemble. This approach enables us to define (time-dependent) averages, and to decide what should be considered to be representative.

It is therefore appropriate to investigate the switching off dynamics in this spirit. The phase-space region of interest is the rectangle  $(-\pi, \pi) \times (-3.2, 3.2)$ . We distribute  $N = 10^5$  points uniformly on it as the initial condition, and follow this ensemble on the stroboscopic map. The set traced out by our ensemble is at any instant of time, after  $t = 10T$ , a snapshot attractor. Its form is *independent* of the initial distribution and of whether the switching off scenario starts at  $t = 10T$  or much later, as the convergence to the attractor at  $C_0 = 2$  requires about  $3T$  only. It should be noted that snapshot attractors are not necessarily chaotic; they can be associated with regular motions, too. A hint on chaoticity might be the filamentary, fractal-like structure of the attractor which signals an underlying horseshoelike structure [1], i.e., a topological identification of chaos. We always initiate the ensemble at time  $t = 0$ , and record its position in the phase space at integer multiples of the period  $T = 2\pi$ .

**A. Attractor geometry changing in time**

The following tableau (Fig. 4) shows the time dependence of the snapshot attractor belonging to a switch-off rate larger than the dissipation rate  $\beta$ . The first panel shows the original chaotic attractor existing yet after  $n = 10$  periods, as the initial shape of the ensemble, at the moment when the

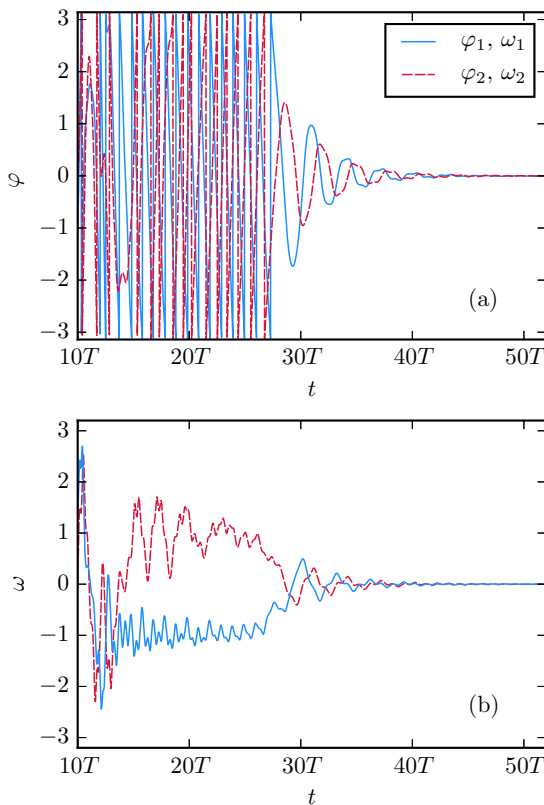


FIG. 3. Single trajectories over the entire switching off process. In panels (a) and (b) the numerically determined angle vs time functions  $\varphi(t)$  and the angular velocity  $\omega(t)$  are displayed for initial conditions  $(\varphi_1 = -1.065, \omega_1 = 1.211)$  continuous (blue) curves and  $(\varphi_2 = -1.071, \omega_2 = 1.185)$  dashed (red) curves, respectively. In both cases, the initial moment is  $t = 10T$ , i.e., the initial conditions are taken on the chaotic attractor right before switching off takes place, with rate  $\alpha = 0.025$ .

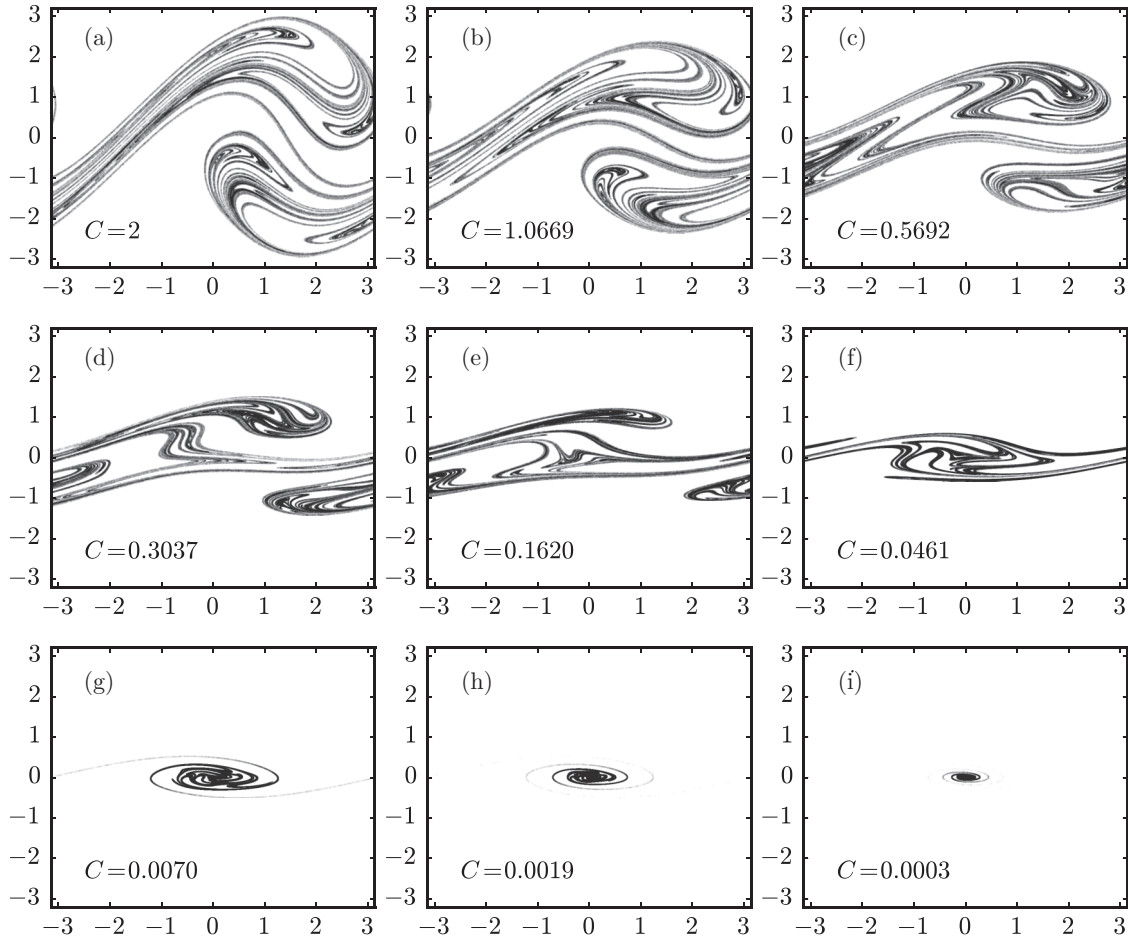


FIG. 4. Snapshot attractors for switch-off rate  $\alpha = 0.1$ .  $N = 10^5$  points are initially evenly distributed over the  $(\varphi, \omega)$  phase space, in the rectangle shown. The snapshot is taken ( $n$  is the number of periods passed since  $t = 0$ ) at  $n = 10$ – $14$  in panels (a)–(e), at  $n = 16$  in (f),  $n = 19$  in (g),  $n = 21$  in (h), and  $n = 24$  in (i). In the panels the corresponding  $C$  values are also indicated.

switching off process starts. The variability of the dynamics is reflected by the extension of the attractor either in the angle or the angular velocity direction (or in both). It is remarkable that filamentarity is present even about ten periods after the beginning of the switching off process [Figs. 4(g) and 4(h)], a time instant for which the amplitude  $C$  fell down to two-thousandths of its original value (cf. Fig. 2).

When comparing with slower scenarios, not shown, a striking difference is that the contraction of the shapes appears to be stronger, at least when considered at the same  $C$  values which, however, belong to much longer times. For faster scenarios filamentary structures remain visible up to smaller  $C$  values since these values are reached during shorter times, and the phase-space contraction due to dissipation cannot yet be pronounced over such short intervals. In other words, the motion remains rather energy rich upon reaching very small  $C$  values in the framework of fast scenarios.

In order to better understand the relationship between the switch-off rates and the dissipation rate, and the expression of this in the snapshot patterns, let us see, for the different scenarios, how the snapshot attractors compare to each other when looked at after a given time  $t$  which is chosen to be on the order of the dissipative relaxation time,  $\tau_d = 1/\beta$ .

When looking at the ensembles after a preselected time, the effect of dissipation is the same for all the scenarios. Thus, the differences in the snapshot attractors are caused by the different switch-off rates themselves. In Fig. 5 all five of the scenarios are presented at time  $t = 25T$ . We immediately see that the smaller switch-off rates display much higher complexity. The one with  $\alpha = 0.05$  is special, because it equals the rate of dissipation,  $\beta$ . We see that for  $\alpha > \beta$ , the ensembles are spiralling near the origin, and for  $\alpha < \beta$  they still very much resemble the initial, chaotic attractor. In other words, the overturning states which stretch over the entire angle range  $2\pi$  seem to disappear for  $\alpha > \beta$  by the time of  $t = 25T$ . Figure 6(d) provides an additional comparison of the different scenarios. Here besides the amplitude ratio  $C(t)/C_0$  the ensemble averaged mechanical energy  $\langle E(t) \rangle / E_0$  is also plotted (symbols) at integer periods [37], where  $E_0$  is the initial average energy. One sees that for fast scenarios the amplitude ratio is below the energy ratio indicating that even after the amplitude has decreased to a negligible small value, the motion is yet rather energetic, and, e.g., overturnings might occur. For slow scenarios small energy values are reached earlier than small values of the amplitude. For  $\alpha = \beta$  (continuous, red curve and diamonds in the last panel) the

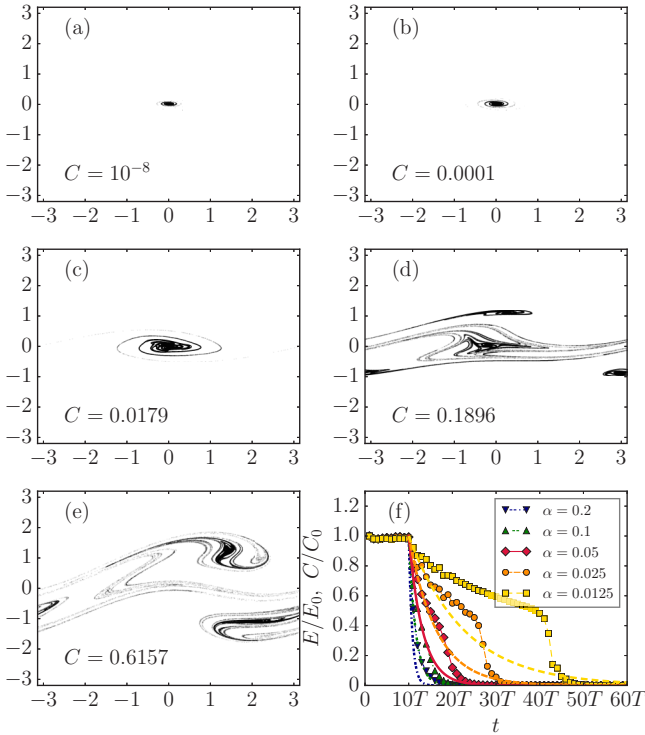


FIG. 5. Snapshot attractors at time  $t = 25T$ , that is 15 periods after the beginning of the switching off process. In panels (a)–(e) the switch-off rates are  $\alpha = 0.2, 0.1, 0.05, 0.025, 0.0125$ . The corresponding amplitudes  $C(t = 25T)$  are also indicated. Panel (f) shows a comparison of the relative amplitude  $C(t)/C_0$  (curves as shown in Fig. 1) and the relative mechanical energy averaged over the ensemble  $\langle E(t) \rangle / E_0$  (symbols), where  $E_0$  is the initial average energy.

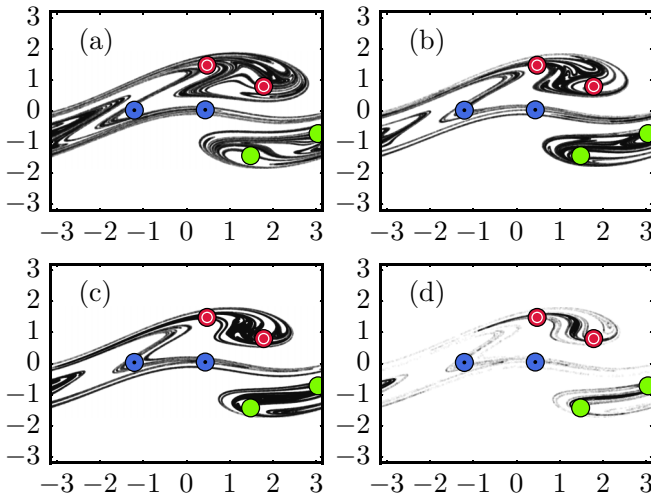


FIG. 6. Comparison of the snapshot attractors with the frozen-in attractors for switch-off rates  $\alpha = 0.1$  (a),  $0.05$  (b),  $0.025$  (c), and  $0.0125$  (d) when the amplitude takes on  $C = 0.5692$ . Colored Dots indicate the coordinates of the frozen-in (regular) attractors for the same  $C = 0.5692$ , marked with the same color as in the bifurcation diagram. The snapshot attractors have *nothing to do* with the frozen-in attractors belonging to the same  $C$  value.

two quantities become negligible at about the same time. This indicates a qualitative difference between fast and slow scenarios: the former dynamics is energetically rich at the end of the switching off process.

### B. Comparison of the snapshot attractors with the frozen-in attractors

We take a fixed  $C = 0.5692$  value where only three simple periodic attractors, period-2 limit cycles, exist. Whatever switch-off rate is chosen, the ensemble when reaching this  $C$  value differs greatly from the frozen-in attractors: the ensemble has a very rich filamentary structure. In Fig. 6 the points (large dots) of the frozen-in periodic attractors do not even overlap with the branches of the snapshot attractor in many instances. Accumulation about these points is strongest for the lowest rate, but even here the filamentary structure stretches over the whole angle range.

### C. Comparison of frozen-in unstable manifolds and the snapshot attractors

The grey dots in Fig. 2(b) provide a clear evidence for the presence of long-lived transients over a broad range of frozen-in  $C$  values. Transient chaos is governed by an underlying nonattracting chaotic set, a chaotic saddle in phase space [38]. As any saddle, it also possesses both a stable and an unstable manifold. The unstable manifold is characteristic for moving away from the chaotic saddle. Since the frozen-in attractors differ strongly from the snapshot attractors, it is natural to compare the latter with the invariant sets of the frozen-in chaotic saddles.

When the driving amplitude is continuously changing, there is no time to reach a particular attractor belonging to a given  $C$  value. The ensemble of trajectories is thus expected to reflect the deviation from chaotic saddles. The question thus arises: what is the relationship between the image of the snapshot attractor and the unstable manifold for the appropriate  $C$  value. The latter can be obtained by standard numerical methods worked out in the theory of transient chaos [38]. The black curves in Fig. 7 illustrate that a qualitative similarity can be observed indeed.

The frozen-in saddles possess also stable foliations. To check if an analogous property holds for the decay of chaos, we have iterated an initial phase-space region with the *time reversed* dynamics of (1). In order to generate the grey (red) curve in Fig. 7(c), we took a small disk of phase-space radius 0.1 with  $N = 10^6$  initial points about the unstable period-1 orbit of small amplitude swingings around the origin (the continuation of the middle (blue) branch in Fig. 2(a)) at  $C_0 = 0.5692$  and iterated them backwards with  $\alpha = 0.025$  up to reaching  $C = 1.067$  after four periods. The filaments plotted in grey red in Fig. 7(c) approximate thus the stable foliation of an unstable period-1 orbit on the snapshot attractor at time  $t = 14T$ . The snapshot attractor at the same time is well approximated by the fourth iterate of a small disk about the small-amplitude-swinging period-1 orbit on the  $C_0 = 2$  attractor, thus the black filaments in this panel can also be considered to be the unstable manifold of a period-1 orbit observed at time  $t = 14T$ . These two foliations together imply

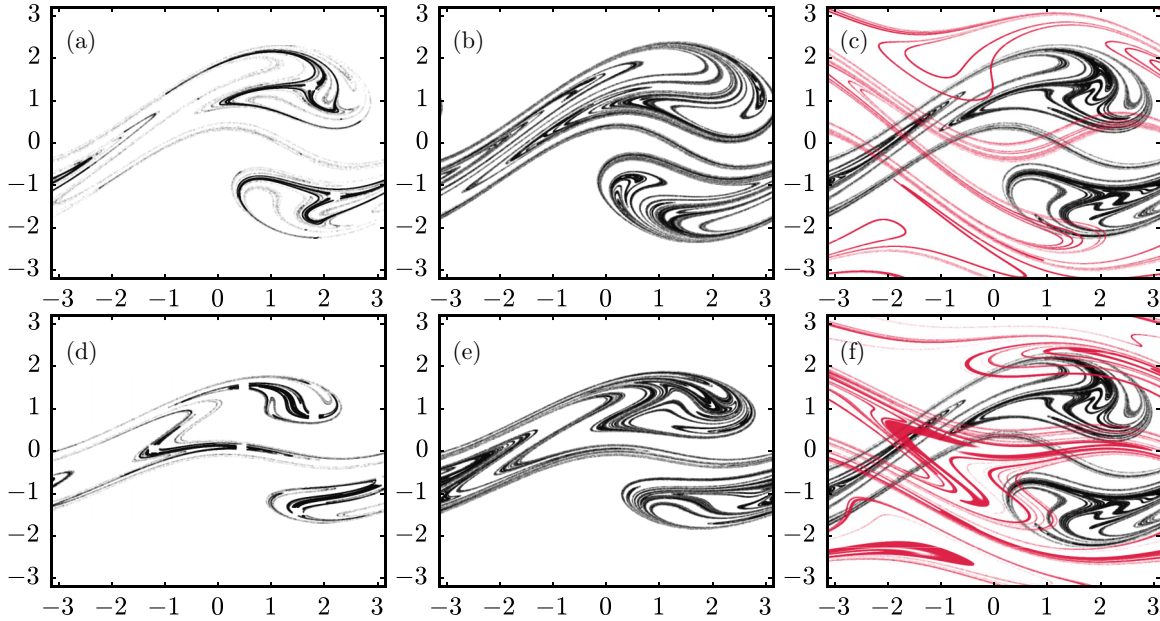


FIG. 7. Comparison of the frozen-in unstable manifold [panels (a) and (d), small rectangles around attractors indicate the escape condition used in the numerics] and the snapshot attractor (b) and (e) reached with  $\alpha = 0.1$  at  $C = 1.0670$  and  $C = 0.5692$ . Panels (c) and (f) exhibit the snapshot attractor for  $C = 1.0670$  and  $C = 0.5692$  with a slow rate,  $\alpha = 0.025$ . In these panels the right column the stable foliation is also given in grey (red) (see text).

the existence of a horseshoe structure in the phase space of even the decaying dynamics, and can be considered a clear indication of chaos. The right lower panel is an analogous stable foliation obtained by taking a small phase-space droplet about the unstable period-1 orbit of small amplitude swingings around the origin at  $C_0 = 0.1620$  and iterating it backwards with  $\alpha = 0.025$  up to reaching  $C = 0.5692$  after eight periods. The dynamics with changing driving might thus also be interpreted as one governed by a continuously moving underlying chaotic saddle, which exists for up to surprisingly low values of  $C$ . (Numerical evidence indicates that in the stable foliation, filamentarity in the droplet's shape never appears when the backward simulation stops at  $C < 0.3$ . Hence no time dependent chaotic saddle can exist in this range.)

## VI. A STATISTICAL MEASURE OF THE DYNAMICS' VARIABILITY

### A. Standard deviation over the ensemble

The internal variability of the dynamics may be characterized by the extent of the attractor either in the angle or in the angular velocity direction. Since the angle is represented in the range  $(-\pi, \pi)$ , this periodic projection is not a proper representation of variability. It is therefore appropriate to concentrate on the angular velocity. The maximum extent of the attractor in this direction may be a good measure of variability. In order to not only reflect a “geometric” property but also take into account the uneven distribution of points on the snapshot attractor, we evaluate the standard deviation of the angular velocity  $\omega$ , that is, the quantity

$$\sigma = (\langle \omega^2 \rangle - \langle \omega \rangle^2)^{1/2}, \quad (4)$$

where the brackets represent averaging over the  $N$  members of the ensemble. This quantity is of course dependent on the time instant  $t$  when the averaging is performed.

Figure 8 shows the  $\sigma(t)$  and  $\sigma(C)$  functions evaluated at integer multiples of the period for the different scenarios. In the  $\sigma(t)$  graph no change can be seen in the first ten periods since the driving is constant  $C_0 = 2$  up to  $t = 10T$ . Immediately after the switching off process starts, for  $t > 10T$ , the standard deviation decreases in time [Fig. 8(a)]. This change is slow, especially for the slow scenarios. The reason for this lies in the existence of transient chaos for a long time in the switching off dynamics. The standard deviation then suddenly drops, indicating a qualitative change in the dynamics, when the region of oscillations about the origin is reached, but the time of the drop depends strongly on the scenario. The  $\sigma(C)$  graphs [Fig. 8(b)] compare the standard deviation in the various scenarios at identical  $C$  values. They are rather similar for  $C > 0.2$ . The region  $C < 0.25$  is blown up in the inset to indicate the dependence of the drop on the scenario. There we see that the scenario with  $\alpha = \beta$  (approximately linear continuous curve with red diamonds) plays the role of a kind of separatrix: fast (slow) scenarios are characterized by approaching zero along a graph with infinite (zero) slope. This indicates again that dynamics with  $\alpha > \beta$  remain rather rich in energy up to very small  $C$  values.

### B. Revival of chaos

Up to now, the dying out of the system's chaotic behavior has been studied. Now we turn to study the process in the reversed direction when the driving amplitude starts growing from an initially small value. It is important to note that this

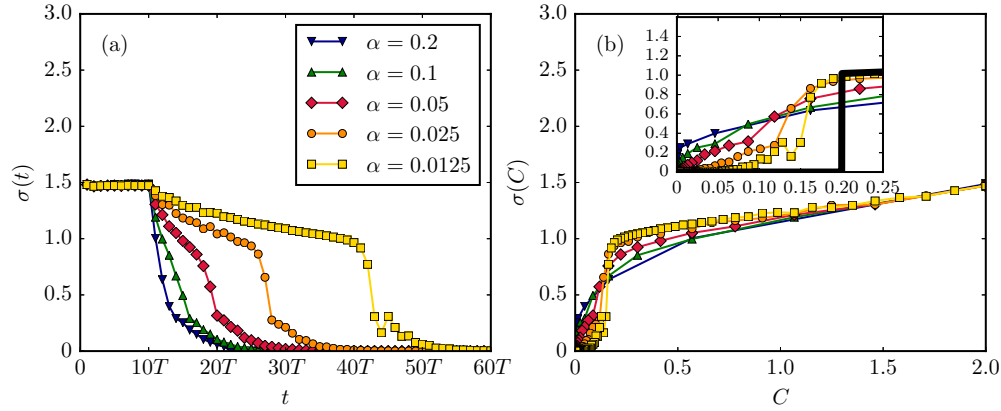


FIG. 8. Standard deviation of the angular velocity  $\omega$  on the snapshot attractor (a) as a function of time and (b) as a function of the amplitude  $C$  (right panel). The ensemble consists of  $N = 10^5$  points, the different scenarios are marked with different symbols. The inset in (b) shows a blow-up of the graphs near the point of a sharp transition, about  $C \approx 0.2$ . The black graph is obtained by evaluating the standard deviation over the periodic orbits of the bifurcation diagram by taking each element with equal weight. This switching over to  $\sigma = 0$  at  $C = 0.2$  is due to the fact that the overturning period-1 attractors disappear in a saddle-node bifurcation here.

is not the time reversed dynamics of Eq. (1). The dynamical problem remains dissipative ( $\beta > 0$ ), Eq. (1) holds, only (2) is replaced by  $C'(t)$  with a formally negative rate (of the same modulus as in the switching off process) and a small initial value  $C^* \ll 1$ :

$$C'(t) = \begin{cases} C^* \cdot e^{\alpha t}, & \text{for } t < t_0^*, \\ C_0, & \text{for } t \geq t_0^*. \end{cases} \quad (5)$$

Time  $t_0^*$  is the length of the switching off process after which the revival starts (see Fig. 9). For function  $C'$  to be continuous,

$$C^* = C_0 e^{-\alpha t_0^*}.$$

For each elapsed period in this new process, the same  $C$  values are obtained, as during the switching off process. The “death,” and “revival” of chaos can thus be compared. Correspondingly, the initial condition for the ensemble of the “revival of chaos” process consists of the snapshot attractor at  $t = 10T + t_0^*$ . Since the initial extension of the ensemble for

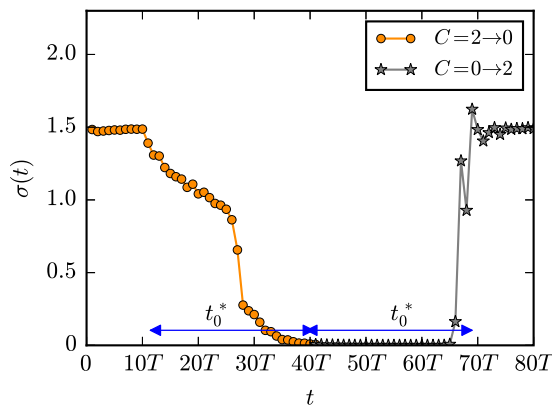


FIG. 9. Time dependence of the standard deviation for the death and revival of chaos. The standard deviation of the ensemble has been calculated according to (4) at the end of each elapsed period. Here  $\alpha = 0.025$ ,  $t_0^* = 30T$ .

the new process is small, the beginning of the ensemble’s time evolution is rather simple, the ensemble remains very much concentrated to the origin. After a few times of ten periods, an increasingly complex pattern appears rather suddenly. The standard deviation of the angular velocity characterizes well the variability of the dynamics in the revival of chaos, too. The results are shown in Fig. 9 such that the data for the revival are plotted as a continuation of the  $\alpha = 0.025$  (orange) curve of Fig. 8(a).

### C. Hysteresis

A different representation of the variability of the death and revival processes is obtained by plotting the results as a function of the instantaneous driving amplitude of both processes on the same plot. The difference between the death and revival of chaos then appears in the form of a *hysteresis* loop. The upper and lower panels of Fig. 10 show the results for the switch-off rate of Fig. 9 and for a much faster scenario, one with  $\alpha = 0.1 > \beta$ , respectively. For the preparation of Fig. 10(b), we took into account that waiting too long would cause the original ensemble to become so much concentrated to the origin that in spite of the increase in the amplitude, the ensemble would numerically remain a point in phase space, with 0 standard deviation. Therefore, here we chose a much shorter  $t_0^*$  value, that of  $12T$ . Comparing the two panels of Fig. 10 we see that the hysteresis loop is more or less of the same size. This is so for all the other scenarios, too. The difference between cases with  $\alpha < \beta$  and  $\alpha > \beta$  is that for slow scenarios the upper curve approaches the origin along the  $C$  axis [as in Fig. 10(a)], while this occurs along the  $\sigma$  axis for fast scenarios [as in Fig. 10(b)], in harmony with the tendency found in the inset of Fig. 8. Further insight can be provided into the mechanisms underlying the hysteresis by plotting the projection of the snapshot attractor on the angular velocity axis, for both the death and the revival process, overlaid with the bifurcation diagram of Fig. 2(b) (see Fig. 11(a)). The fact that the increase in the hysteresis loop starts in all cases at about  $C = 1$  might be related to the collision of the unstable swinging orbit, the continuation of

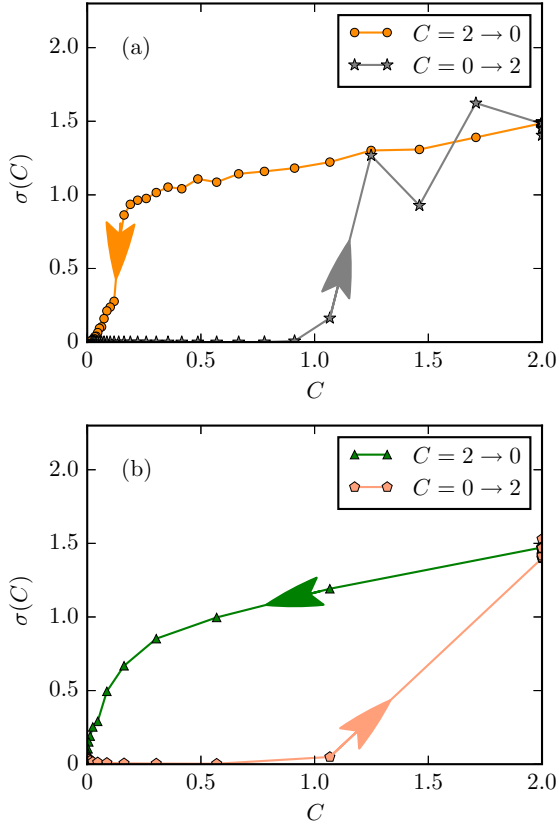


FIG. 10. Panel (a): hysteresis in  $\sigma(C)$  for  $\alpha = 0.025 < \beta$ ,  $t_0^* = 30T$ . Panel (b) for  $\alpha = 0.1 > \beta$ ,  $t_0^* = 12T$ .

the blue branch in the bifurcation diagram, with an extended chaotic saddle at about  $C = 1$ . In the other direction, when  $C$  is decreasing from  $C_0 = 2$ , the ensemble size practically follows the hull of the extension of the chaotic saddle and its unstable manifolds as long as they exist. Our simulations indicate that transient chaos is not present in the frozen-in system for  $C < C_c$ , where  $C_c \approx 0.33$ . This observation also

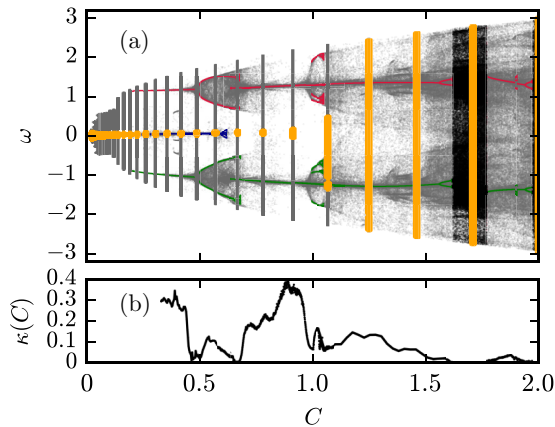


FIG. 11. (a) The extension of the snapshot attractor in the angular velocity direction overlaid with the  $\omega$  vs  $C$  bifurcation diagram [Fig. 2(b)]: revival of chaos (death of chaos) light grey, orange, (dark grey) intervals.  $\alpha = 0.025$ . (b) estimated escape rate of the frozen-in chaotic saddle for the different amplitudes.

explains why the  $\sigma(C)$  curves are practically the same for  $C > 0.33$ . To prepare the discussion of the next section, we display, in Fig. 11(b), the estimated value  $\kappa(C)$  of the escape rate from the frozen-in chaotic saddle. Since the reciprocal of the escape rate sets the average lifetime of transient chaos, we see that the latter extends over a very broad range, in particular since  $\kappa$  approaches zero about crisis points.

VII. DISCUSSION

We have shown that the disappearance of chaos due to the gradual switching off of the driving is a surprisingly complex process. Individual trajectories vary considerably, thus, no single randomly selected time series can be considered to be representative. Therefore, monitoring an ensemble of trajectories (of snapshot attractors) is found to be appropriate. The shape of the attractor itself, and its change in time depends on the switching off scenario.

Naively one might think that the behavior seen during this process is closely related to the bifurcation diagram, which displays the attractors observed in an infinitely slow, quasistatic switching off scenario.

The dynamics studied are found instead to follow roughly the structure of the bifurcation diagram containing the transients: the unstable manifolds of the underlying frozen-in chaotic transients are observed to be reflected in the patterns of snapshot attractors. This suggests that a portion of the ensemble members may come close to some chaotic-saddle-like structures, but because they are unstable, trajectories start moving away from there along the unstable manifolds. There is not enough time for the trajectories to reach the frozen-in attractor, because the driving is ever shifting in time. Not even the frozen-in unstable manifolds lead to total agreement. We have seen that below  $C_c \approx 0.33$  no transient chaos can exist in the frozen-in system, but the snapshot attractor of Fig. 4(f) belonging to  $C = 0.0461$  has a strong filamentary structure. A possible explanation might be here that by reaching this  $C$  value, due to the previously existing chaotic saddle, and its manifolds, the snapshot attractor already has a striated structure. Later this shape is just passively “advected” further in the phase space, which is now lacking any kind of frozen-in chaos. We thus conclude that the death of chaos can only start below the critical  $C_c$  value which designates the disappearance of transient chaos in the frozen-in system.

Our observations help to formulate what the condition for a “quasistatic” switching off is. Without knowing chaos theory one may think that the switch-off time must be much longer than the dissipative relaxation time:  $\tau_s \gg \tau_d$ . However, transient chaos defines a new timescale which is estimated by the reciprocal of the escape rate from the chaotic saddle,  $1/\kappa$ . This can be much larger than the dissipative relaxation time. In addition, the escape rate may depend on all parameters of the nonlinear problem. The condition for a quasistatic process becomes thus

$$\alpha \ll \beta, \kappa_{\min}, \tag{6}$$

where  $\kappa_{\min}$  is the lowest value in the whole range of parameters tested. In our case  $\beta = 0.05$ , and the minimum of the numerically determined escape rates [Fig. 11(b)] is very small

(at crises points the theoretical value of  $\kappa$  is exactly zero). We thus conclude that a quasistatic switching off is impossible over the full range (0,2) of driving amplitudes. The dynamics of the switching off process is much richer than any frozen-in dynamics.

Finally, we note that the driven pendulum is of course only one, but a generic, example. In practically the same spirit, we can also find a condition for quasistatic switching off in cases where the phase-space contraction and the switching off scenarios follow a general time dependence. In this case, for every moment, that is, for each value of  $C$  during the scenario, we can define an effective  $\beta(C)$  and  $\alpha(C)$  parameter belonging to that  $C$ . These are to be compared with the escape rate for the particular frozen-in  $C$  value. The local condition for a quasistatic scenario becomes then to be

$$\alpha(C) \ll \beta(C), \kappa(C), \quad (7)$$

for any possible  $C$  value. In our example there are  $C$  intervals where  $\kappa(C) > \beta$ , but the condition  $\alpha \ll \beta$  is never fulfilled

since the smallest  $\alpha$  is just one-quarter of  $\beta$ . This explains *a posteriori* why we never found a good agreement with the bifurcation diagram, and this is why the black curve of the inset of Fig. 8(b) is not reached by our numerical data. The problem of understanding the dynamics in the presence of a driving subjected to a temporal shift is very general, and might occur in many disciplines, in particular in our era of climate change. The details may vary from case to case, but it is generally true that the switching off dynamics with a naturally chosen switch-off scenario *cannot* be deduced from the frozen-in cases.

#### ACKNOWLEDGMENTS

We benefitted from useful discussions with G. Drótos and C. Kuehn. T.T. is grateful for support from the Alexander von Humboldt Foundation. This work was also supported by the Hungarian Science Foundation under Grant No. NK100296. U.F. is grateful for support from the Hungarian Academy of Sciences.

- 
- [1] E. Ott, *Chaos in Dynamical Systems* (Cambridge University Press, Cambridge, England, 1993).
  - [2] T. Tél and M. Gruiz, *Chaotic Dynamics* (Cambridge University Press, Cambridge, England, 2006).
  - [3] J. Argyris, G. Faust, M. Haase, and R. Friedrich, *An Exploration of Dynamical Systems and Chaos* (Springer, New York, 2015).
  - [4] T. Parker and L. Chua, *Practical Numerical Algorithms for Chaotic Systems* (Springer-Verlag, New York, 1989).
  - [5] C. Baesens, *Physica D* **53**, 319 (1991).
  - [6] T. Erneux and P. Mandel, *Opt. Commun.* **85**, 43 (1991).
  - [7] R. Haberman, *Chaos* **10**, 641 (2000).
  - [8] S. M. Baer and E. M. Gaekel, *Phys. Rev. E* **78**, 036205 (2008).
  - [9] Y. Park, Y. Do, and J. M. Lopez, *Phys. Rev. E* **84**, 056604 (2011).
  - [10] P. Ashwin, S. Wicczorek, R. Vitolo, and P. Cox, *Philos. Trans. R. Soc. London, Ser. A* **370**, 1166 (2012).
  - [11] S. Wicczorek, P. Ashwin, C. M. Luke, and P. M. Cox, *Proc. R. Soc. London, Ser. A* **467**, 1243 (2011).
  - [12] P. Ashwin, C. Perryman, and S. Wicczorek, [arXiv:1506.07734](https://arxiv.org/abs/1506.07734).
  - [13] C. Kuehn, *Multiple Time Scale Dynamics* (Springer, New York, 2015).
  - [14] M. Ghil, M. D. Chekroun, and E. Simonnet, *Physica D* **237**, 2111 (2008).
  - [15] R. Serquina, Y.-C. Lai, and Q. Chen, *Phys. Rev. E* **77**, 026208 (2008).
  - [16] M. D. Chekroun, E. Simonnet, and M. Ghil, *Physica D* **240**, 1685 (2011).
  - [17] T. Bódai and T. Tél, *Chaos* **22**, 023110 (2012).
  - [18] G. Drótos, T. Bódai, and T. Tél, *J. Clim.* **28**, 3275 (2015).
  - [19] F. J. Romeiras, C. Grebogi, and E. Ott, *Phys. Rev. A* **41**, 784 (1990).
  - [20] L. Arnold, *Random Dynamical Systems* (Springer, New York, 1998).
  - [21] P. Kloeden and M. Rasmussen, *Nonautonomous Dynamical Systems*, Mathematical Surveys and Monographs No. 176 (American Mathematical Society, Providence, 2011).
  - [22] A. N. Carvalho, J. A. Langa, and J. C. Robinson, *Attractors for Infinite-Dimensional Nonautonomous Dynamical Systems*, Applied Mathematical Sciences No. 182 (Springer, New York, 2013).
  - [23] L. Yu, E. Ott, and Q. Chen, *Phys. Rev. Lett.* **65**, 2935 (1990); *Physica D* **53**, 102 (1991).
  - [24] J. C. Sommerer and E. Ott, *Science* **259**, 335 (1993).
  - [25] J. Jacobs, E. Ott, T. Antonsen, and J. Yorke, *Physica D* **110**, 1 (1997).
  - [26] Z. Neufeld and T. Tél, *Phys. Rev. E* **57**, 2832 (1998).
  - [27] J. L. Hansen and T. Bohr, *Physica D* **118**, 40 (1998).
  - [28] G. Károlyi, T. Tél, A. P. S. de Moura, and C. Grebogi, *Phys. Rev. Lett.* **92**, 174101 (2004).
  - [29] T. Bódai, G. Károlyi, and T. Tél, *Phys. Rev. E* **83**, 046201 (2011).
  - [30] A. Pikovsky, in *Nonlinear and Turbulent Processes in Physics*, edited by R. Z. Sagdeev (Harwood Academic, Reading, 1984), Vol. 3; *Radiophys. Quantum Electron.* **27**, 576 (1984).
  - [31] J. D. Daron and D. A. Stainforth, *Environ. Res. Lett.* **8**, 034021, (2013); *Chaos* **25**, 043103 (2015).
  - [32] W. L. Ku, M. Girvan, and E. Ott, *Chaos* **25**, 123122 (2015).
  - [33] M. Herein, J. Márffy, G. Drótos, and T. Tél, *J. Climate* **29**, 259 (2016).
  - [34] S. Pierini, M. Ghil, and M. Chekroun, *J. Clim.* **29**, 4185 (2016).
  - [35] A. Hadjighasem, M. Farazmand, and G. Haller, *Nonlinear Dyn.* **73**, 689 (2013).
  - [36] G. Drótos, T. Bódai, and T. Tél, *Phys. Rev. E* **94**, 022214 (2016).
  - [37] The mechanical energy at any time instant  $t$  is  $E = \dot{\varphi}^2/2 - \gamma^2(\cos \varphi - 1) + A^2 \sin^2 t - 2A \sin t \sin \varphi$ .
  - [38] Y.-C. Lai and T. Tél, *Transient Chaos* (Springer, New York, 2011).